VII International Conference on Computational Methods in Marine Engineering
MARINE 2017
M. Visonneau, P. Queutey and D. Le Touzé (Eds)

IMPROVED MODELLING OF SHEET CAVITATION DYNAMICS ON DELFT TWIST11 HYDROFOIL

Guilherme Vaz[1], Thomas Lloyd[1] and Arun Gnanasundaram[2]

[1]MARIN
Haagsteeg 2, Wageningen 6708 PM, The Netherlands
e-mail: {g.vaz; t.lloyd}@marin.nl

[2]TU Delft
Kluyverweg 1, Delft 2629 HS, The Netherlands
e-mail: A.K.Gnanasundaram@student.tudelft.nl

Key words: Delft Foil, Cavitation, RANS, Reboud-correction, DDES, ReFRESCO

Abstract. In this paper, unsteady viscous-flow cavitation predictions for a 3D hydrofoil are performed using three different approaches: 1) a pure RANS method; 2) a RANS method including an eddy-viscosity "Reboud" correction; 3) a DDES Scale-Resolving-Simulation approach. Both wetted and cavitating flow conditions are analysed and compared with experimental data. The accuracy of these approaches is scrutinised in terms of integral quantities, cavity dynamics, different background principles, and the influence of grid refinement. Low numerical uncertainties have been obtained for wetted flow conditions, but a somewhat large deviation on the wing loading has been observed when compared with experimental results. For the cavitating flow case, the RANS calculations do not accurately simulate the cavity dynamics. The RANS-Reboud correction improves the fidelity of the calculations at increased numerical demands and decreased robustness. The DDES approach leads to improved dynamics, slightly less accurate cavity shedding mechanism, at lower computational cost. The cavity extents are underpredicted for all methods and conditions used, when compared with the available experimental data.

1 INTRODUCTION

Cavitation occurs when the static pressure of the liquid drops below its corresponding saturation pressure leading to the formation of vapour. This often occurs near the leading edge of the blades of devices such as propellers and pumps. Part of this vapour then breaks off from the leading edge, convects downstream, and undergoes condensation. The process of vapour shedding imposes fluctuating loads on the blades, while the collapse of the vapour leads to erosion of the surface of blades. Associated pressure fluctuations and noise generation are also often an issue. Hence the susceptibility of a propeller design to cavitation must be understood during the design stage, which has led to research attention focussing on the computational modelling of cavitation. It has been noted however that the interactions between the vapour and the tur-

bulence structures reveal some complexities which make it challenging to capture the cavitation mechanism accurately using common engineering numerical modelling approaches [1].

Cavitating flow simulations are very sensitive to the turbulence and cavitation models used. Traditional Reynolds-averaged Navier-Stokes (RANS) models tend to overpredict the turbulent viscosity in the cavity closure region, dampening the turbulent interactions that promote shedding. This has been well established in [2, 3]. As put forth in [4], a way to overcome this deficiency is by using *ad hoc* corrections to reduce the turbulent dissipation in those regions, allowing the vapour to grow and shed from the leading edge. Though the effectiveness of this correction in promoting shedding with different turbulence models have been demonstrated [1, 3, 5], the influence of grid resolution effects and discretisation errors on the cavitation solution have not received as much attention.

The failure of standard RANS models to accurately capture the unsteady phenomenon of cavitation is not surprising, since these were not originally designed for multiphase unsteady flows. On the other hand, Scale-Resolving Simulations (SRS) are expected to give a better prediction of reality. Large-Eddy Simulations (LES) and Delayed-Detached Eddy Simulations (DDES) restrict the extent of modelled turbulence, thereby reducing the modelling error. SRS performed in [3], [6] and [7] report the improvement in the predictions and show increased cavity length and shedding frequencies that match more closely with experiments than RANS. [3] and [8] also provide comparisons between RANS and SRS, but limit themselves to a quantitative comparison of the mean lift coefficient, vapour volume, and shedding frequency. In this paper, we aim to analyse the differences between the application of SRS (more specifically the DDES formulation), RANS and RANS including eddy-viscosity correction for unsteady cavitation predictions. We analyse their numerical requirements, different background principles with respect to cavitation dynamics, and the influence of numerical errors on their working behaviour.

The chosen test case is the well-known Delft 'Twist11' Foil, for which experimental results from [9] and [10] are available for use as validation material, while comparison can also be made to numerous computational results from the open literature. The numerical approach taken, the discretisation schemes, and a brief description of the solver used in this work is covered in Section 2. Details of the grids generated for the study, the computational domain and numerical settings adopted are given in Section 3. Results of the wetted and cavitating flow simulations are included in Section 4. Finally, concluding remarks are made in Section 5.

2 SOLUTION METHOD

2.1 Flow solver

The governing equations were solved using a finite volume viscous-flow CFD code ReFRESCO (www.refresco.org) developed at MARIN, Technical University of Delft and several other universities around the world. The equations are solved in a segregated manner and the coupling happens iteratively using a SIMPLE-type algorithm. A second order QUICK scheme was used for discretisation of convective fluxes in the momentum equation, with a flux limiter activated to provide numerical stability. For fluxes in the turbulence equation and the transport equation for cavitation, a first-order upwind scheme was used. A second-order implicit time marching scheme was used.

2.2 Turbulence and cavitation modelling

For RANS simulations the $k-\sqrt{k}L$ model for turbulence [11] was used. This model predicts lower levels of eddy viscosity (ν_t) than the more commonly-used $k-\omega$ SST model, and has been shown to improve prediction of cavitation dynamics for propellers [12]. For some simulations, this model was combined with the viscosity correction proposed in [4] (and thereafter referred as Reboud correction), which reads as

$$f(\alpha) = \rho_v + \left(\frac{\rho - \rho_v}{\rho_l - \rho_v}\right)^n (\rho_l - \rho_v) = \rho_v + (1-\alpha_v)^n (\rho_l - \rho_v), \quad n \geq 1, \tag{1}$$

where α is the volume fraction, ρ is the mixture density and the subscripts l and v refer to liquid and vapour values respectively. The parameter n must be chosen, with the authors of the correction recommending that 10 be used. The function $f(\alpha)$ is used to correct the magnitude of the eddy viscosity predicted by the turbulence model $\mu_t = \mu_t^* f(\alpha)/\rho$, with $\mu_{eff} = \mu + \mu_t$ being the effective mixture viscosity used in the diffusion term of the momentum equations.

Scale resolving simulations (SRS) were performed using Delayed Detached Eddy Simulations (DDES) based on the $k-\omega$ SST model [13]. DDES aims to resolve turbulent structures in separated flow regions and switches to RANS in regions where the mesh size is not large enough to capture the small scale structures, as well as in near-wall regions (enforced). The switch between RANS and LES for DDES is determined based on a localised length scale (l_t) given as

$$l_t = l_{RANS} - f_d \max(l_{RANS} - l_{LES}, 0), \tag{2}$$

where l_{RANS} is the turbulent length scale of the $k-\omega$ SST model, f_d is a blending function and $l_{LES} = C_{DES}\Delta$ is the LES length scale based on the local cell size $\Delta = max(\Delta x, \Delta y, \Delta z)$. l_t is then used to decrease the destruction of k of the SST model, and therefore decrease μ_t.

Cavitation was modelled by considering a homogeneous mixture of liquid and vapour bubbles. A transport equation for the vapour volume fraction α_v is solved, with the source term based on the square root of the difference between the local and saturation pressure according to [14] (Sauer model). The slight modifications to the source term proposed by [15] were also used.

3 COMPUTATIONAL SETUP

3.1 Computational domain and boundary conditions

The Delft Foil is a twisted hydrofoil with a NACA0009 profile and has a spanwise varying angle of attack (AoA) from 0° at the sides to 11° at the midspan. The foil has a chord length (c) of 0.15 m, and is placed at an AoA of $-2°$. The domain inlet was located $2c$ upstream of leading edge (LE) of the foil, and extends to $5c$ downstream. The x-axis was aligned with the flow, while the y-axis extended in the spanwise direction from 0 to b (the foil halfspan, equal to c) with a symmetry condition imposed on the midspan plane. The top and the bottom walls were both located one chord from the foil. A no-slip condition was imposed on the foil surface, while the side walls were treated as slip walls. An inflow boundary condition was specified at the inlet, while at the outlet a fixed zero pressure was used. The computational domain is shown in Figure 1.

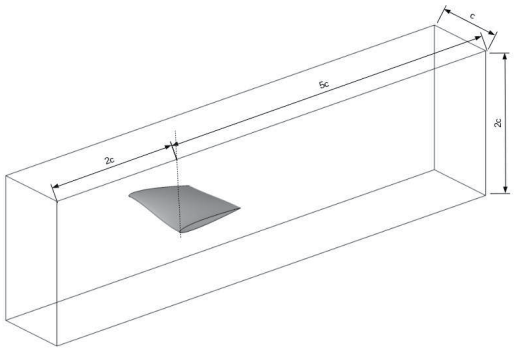

Figure 1: Computational domain for halfspan Delft Twist11 Foil case.

Table 1: Summary of grid statistics for all halfspan grids.

grid	no. of cells / M	target y^+_{max}
G2	4.50	0.40
G3	2.10	0.50
G4	1.30	0.65
G5	0.42	0.80

3.2 Grids

Four block structured grids were generated using *GridPro*, by successively coarsening the finest grid by a factor of 1.25. The total number of cells and targeted maximum normalised wall-normal cell height y^+_{max} are listed in Table 1. The resulting grids are geometrically similar allowing systematic analysis of the effect of grid refinement on the flow solution.

In order to adapt the grids somewhat for cavitation prediction, cells were concentrated on the suction side of the foil, including in the region where shed cavitation was expected, as well as towards the midspan of the foil (symmetry plane of the domain). It was also expected that this topology would help in the resolution of shed vortices when performing DDES. Figure 2 clearly shows the grid density in this region.

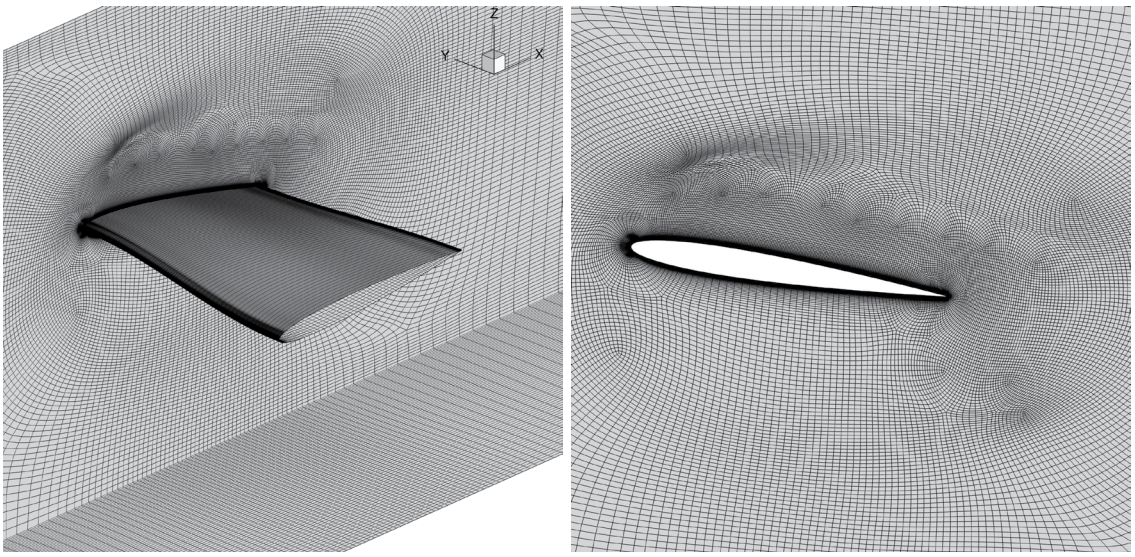

Figure 2: Views of grid G3: (left) perspective view of the foil; (right) slice at symmetry plane.

3.3 Computational settings

The chosen test conditions correspond to those frequently seen in the literature for numerical computations of the geometry. Velocity at the inlet was prescribed as U_0=(6.97, 0, 0) ms^{-1}, with inlet values for the turbulence quantities set in order to give a turbulence intensity of 1%. The pressure at the outlet was fixed at $p_0 = 0\ Pa$. Wetted flow steady simulations were performed by setting p_v to avoid the formation of vapour. Both RANS ($k - \sqrt{k}L$ based) and DDES ($k - \omega\ SST$ based) were performed. In steady attached flow, these DDES calculations are almost pure RANS. The solution was considered to be well converged once the L_∞-residuals reached 1×10^{-9}. A wetted flow solution served as starting point for cavitating flow simulations with cavitation introduced in steps by adjusting the vapour pressure p_v to achieve the correct cavitation number, which was $\sigma = 1.07$, with $\sigma = 2(p_0 - p_v)/(\rho_l U_0^2)$.

Both liquid and vapour values for the fluid densities and dynamic viscosities were specified *viz.* $(\rho_l, \rho_v) = (998, 0.024)\ kgm^{-3}$ and $(\mu_l, \mu_v) = (100.2, 1.02) \times 10^{-5}\ kgm^{-1}s^{-1}$. For the cavitation model, the number of nuclei per unit volume was set to 10^8 while the minimum bubble radius was restricted to $1 \times 10^{-5}\ m$. Finally, the Reboud parameter which controls the magnitude of the eddy viscosity correction was chosen as $n = 4$, much lower than typically used in the literature. This value was used due to the fact that the eddy viscosity level for the $k - \sqrt{k}L$ model was expected to be several times lower than would be predicted using the $k - \omega\ SST$ model.

RANS cavitating-flow calculations were performed using a normalised timestep $\Delta t^* = \Delta t U_0/c$ of 2.3×10^{-3}, while $\Delta t^* = 7 \times 10^{-4}$ was used for DDES simulations. The lower timestep for DDES was chosen aiming to improve the temporal resolution of the scale-resolved part of the flow such that the affect of grid size was more important than timestep. For RANS computations with Reboud correction, the number of outer loops had to be increased with the number of grid cells in order to achieve sufficient iterative convergence within each timestep.

4 RESULTS & DISCUSSION

4.1 Wetted flow simulations

Comparison of wetted flow simulations are made in terms of the lift, drag and pressure coefficients, defined as $C_L = 2L/(\rho_l cb U_0^2)$, $C_D = 2D/(\rho_l cb U_0^2)$ and $C_p = 2(p - p_0)/(\rho_l U_0^2)$. Here L and D are the forces perpendicular to and parallel to the inflow direction, and cb is the foil planform area. An uncertainty analysis using the method proposed in [16] was performed to assess the discretisation uncertainty (U) for the RANS calculations. Note that for DDES, even in steady attached flow, the LES/DDES branch is activated in the wake of the wing. Moreover, in DDES the modelling error is entangled with the numerical error due to the grid-dependent l_{LES} filter, and therefore the V&V method of [16] cannot be applied.

The differences in C_L between the finest and the coarsest grid in RANS and DDES simulations are less than 0.6% and 0.8% respectively. The corresponding values for C_D are even smaller for both turbulence models. For the finest grid (G2) the RANS results are 0.425 for C_L and 0.0146 for C_D, while for DDES these are 0.428 and 0.0143 respectively. The associated uncertainty U for the RANS calculations is 1.0% for C_L and 1.5% for C_D. Even if it has been recognised in

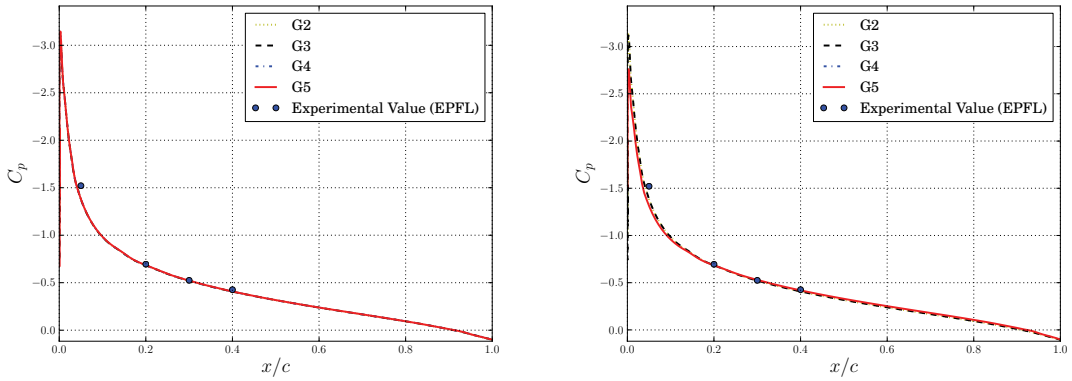

(a) RANS (b) DDES

Figure 3: Pressure coefficient on foil surface at $y/b = 0.5$ (midspan plane) for RANS and DDES computations using all grids. Experimental values from [9].

the literature that a high uncertainty exists on the experimental lift value of 0.47[1], one should emphasise that the numerical results here presented deviate by more than 9% from this value.

The non-dimensionalised pressure on the foil along the midspan plane is plotted alongside experimental data from [9] in Figure 3. A good agreement is observed between the two data sets, while the sensitivity of the surface pressure distribution to grid density is seen to be small.

4.2 Cavitating flow simulations

4.2.1 Flow fields

Figure 4 illustrates a general overview of the cavity layout (represented by an iso-surface value of $\alpha_v = 0.1$), together with limiting streamlines, and contours of eddy-viscosity, for the three approaches here employed. Figure 5 shows axial velocity and off-plane vorticity fields at the symmetry plane (halfspan), together with a vapour contour of $\alpha_v = 0.1$.

These instantaneous flow fields show that the cavity predicted by a pure RANS solution is small. Also, the eddy-viscosity exhibits high values inside and downstream of the cavity as well as in the wake at the symmetry plane, the most highly-loaded section of the wing. The limiting streamlines show backward flow inside but also downstream of the cavity. The flow is steady, mostly two-dimensional and there is a small re-entrant jet, but no side re-entrant jets. With RANS-Reboud the cavity sheds and the flow is highly unsteady. Inside the cavity and shed vapour pockets the eddy-viscosity is reduced; but around these structures, or associated shed vortical structures without vapour, the eddy-viscosity values are high. The limiting streamlines inside the cavity are more chaotic, and both side and longitudinal re-entrant jets can be seen. Figure 5 shows more clearly the re-entrant jet present in both approaches, and the more complex structures both in terms of vapour pockets and vortices in the DDES results.

[1] Corroborated by Evert-Jan Foeth [17].

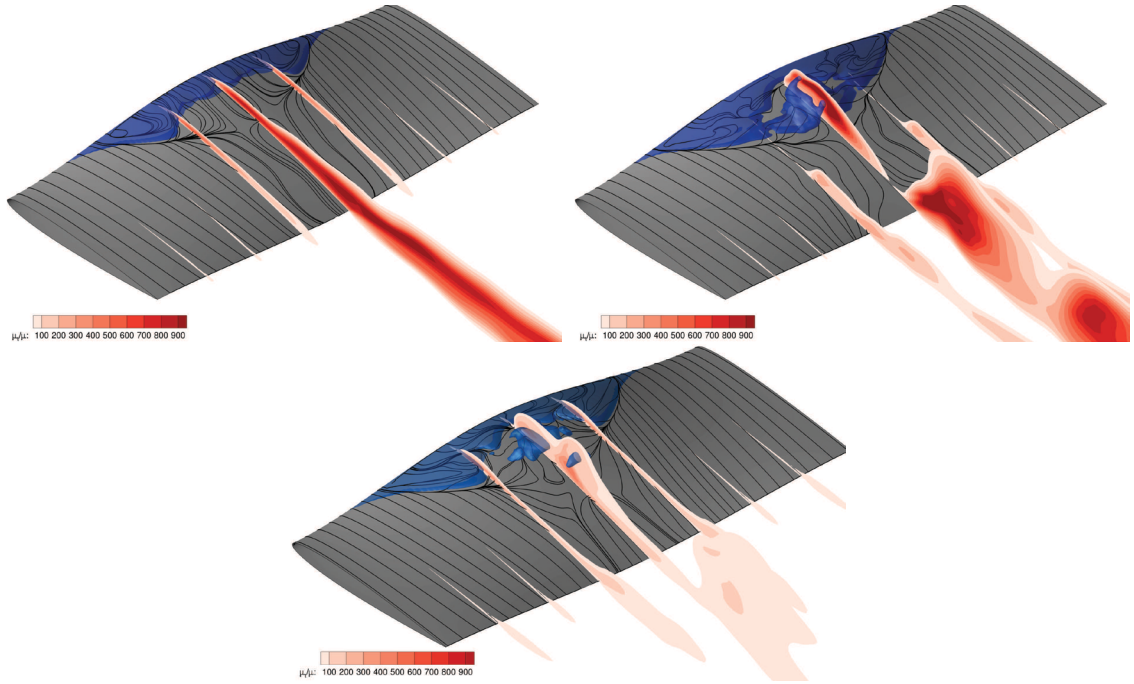

Figure 4: Cavity extent, limiting-streamlines and eddy-viscosity field. Instantaneous values. RANS (top-left), RANS-Reboud (top-right) and DDES (bottom).

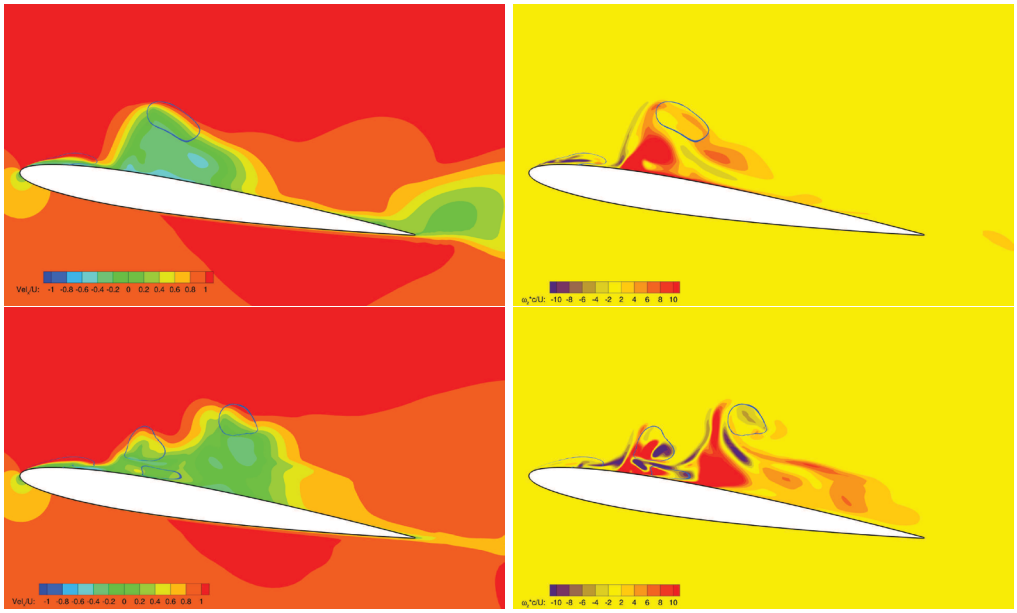

Figure 5: Axial velocity field (left), off-plane vorticity field (right) and cavity contour ($\alpha_v = 0.1$). Instantaneous values on symmetry plane. RANS-Reboud (top) and DDES (bottom).

4.2.2 Effect of grid resolution

Figure 6 shows values of $\overline{C}_L$, Strouhal number St (defined as $St = fc/U_0$ where f is the main shedding frequency) and total vapour V_v obtained for the current simulations and grids, together with results available in the literature. Figure 7 presents the time history of lift and vapour *vs* the grids used. Figure 8 shows the effect of the grid resolution on the cavity layout, limiting streamlines and eddy-viscosity values.

As also seen in the previous section, the RANS simulations give a grossly underpredicted cavity, which only extends until about 20% of the chord ($l/c = 0.2$), and remains attached to the foil surface. The dynamics does not improve with grid resolution; in fact, the results reach (almost) steady state with V_v becoming constant and reducing with increasing grid resolution. Application of the Reboud correction has a large effect on the flow solution. A value of $n = 4$ almost doubles the length of the cavity, and the lift also increases. The time histories of V_v and C_L in Figure 7 show that significant cavitation dynamics also result, yielding a St of around 0.7, as in the experiments. Grid refinement has a somewhat non-monotonic behaviour both in terms of on lift and total vapour volume, showing the existence of possible numerical issues. As stated previously, the number of non-linear outer-loops had to be increased significantly for RANS-Reboud with increasing grid resolution. Nevertheless, in general, one can say that the cavities are larger and have a larger volume with increasing grid resolution. The peaks seen in the lift curve are due to the condensation/collapse phase of the cavity, and have been reported several times in the literature by other authors, specially when using the Sauer cavitation model.

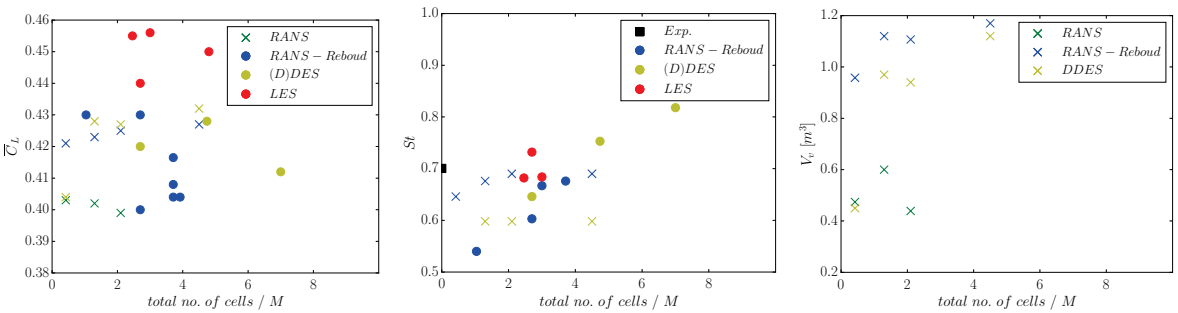

(a) Lift coefficient (b) Strouhal number (c) Vapour volume

Figure 6: Mean C_L, St and V_v variation with total number of grid cells for RANS, RANS-Reboud, (D)DES and LES cavitating flow simulations. Crosses denote results from the present study, while circles show results from literature.

The DDES results yield slightly higher C_L but lower St and vapour volumes than those using RANS-Reboud. The time histories of the lift and vapour volume show a more monotonic and well-behaved convergence with grid refinement. In DDES, the finer the grid, the more turbulent structures are being solved, and the larger the dynamic behaviour of the solution. Also, it is interesting to note that for the coarsest grid G5 DDES leads to steady results. On the contrary, for the same grid, even a "simpler" RANS solution (not shown here) leads to shedding

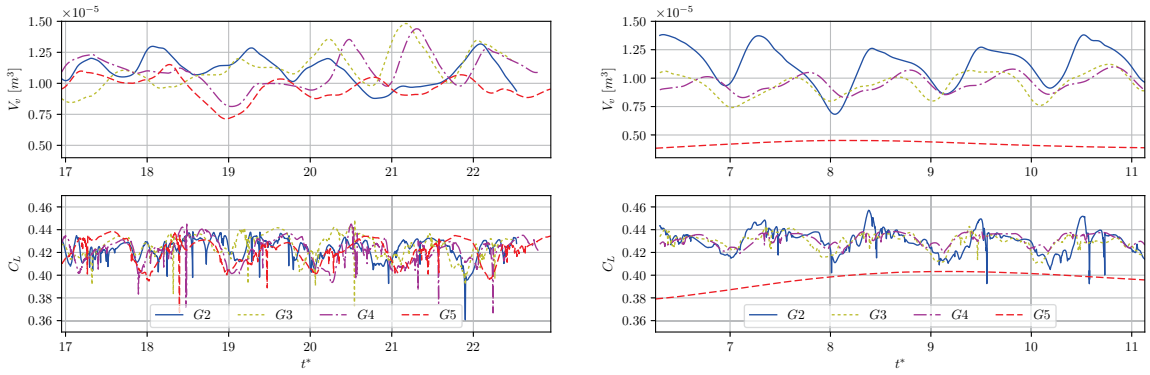

(a) RANS-Reboud (b) DDES

Figure 7: Time histories of C_L and V_v for RANS-Reboud and DDES cavitating flow simulations, showing effect of grid refinement.

and dynamic behaviour. Figure 8 shows that grid refinement reduces the eddy-viscosity and increases the vapour pockets shed, in both RANS-Reboud and DDES cases.

The comparison of the present results with the ones available in the literature show similarities on St, with values around 0.70. However, for C_L the spread is larger with variations more than 10%. It is also interesting to note that the total vapour volume is rarely reported in the literature, and that the grids used in the current work for the halfspan wing are similar in terms of resolution to the ones used by some authors for the complete wing.

4.2.3 Cavity dynamics

In order to further study the working principles of the Reboud correction and DDES on cavitating flow dynamics, Figure 9 presents the instantaneous eddy-viscosity field, Reboud correction $f(\alpha)/\rho$, with $f(\alpha)$ defined by Equation 1, and DDES activation region $1 - \frac{l_t}{l_{RANS}}$, with l_t defined by Equation 2, at the symmetry plane computed using the finest grid G2.

The eddy-viscosity levels are significantly reduced in the DDES calculations for the complete plane, while the Reboud correction decreases these levels only inside the cavitation/vapour areas. The lower left part of Figure 9 shows the values of $f(\alpha)/\rho$ for the same time instant, showing that this correction is only active within vapour zones. The lower right part of Figure 9 shows that even for G2, with 4.5M cells for the halfspan wing, the values of $1 - \frac{l_t}{l_{RANS}}$ are still too high (always larger than 0.5), and that due to the DDES intrinsic boundary-layer shielding, the LES mode is not activated within vapour areas inside the boundary-layer. This affects the re-entrant jet dynamics and the associated overall shedding mechanism. It is believed that grid refinement, especially in the longitudinal and transverse directions will slightly improve this issue, but not solve it. Other SRS models, for instance XLES, IDDES or PANS, which are allowed to solve turbulence anywhere in the flow field are needed, and the authors are of the opinion that for these same reasons wall-modelled LES models will not be completely effective for this type of cavitating flow.

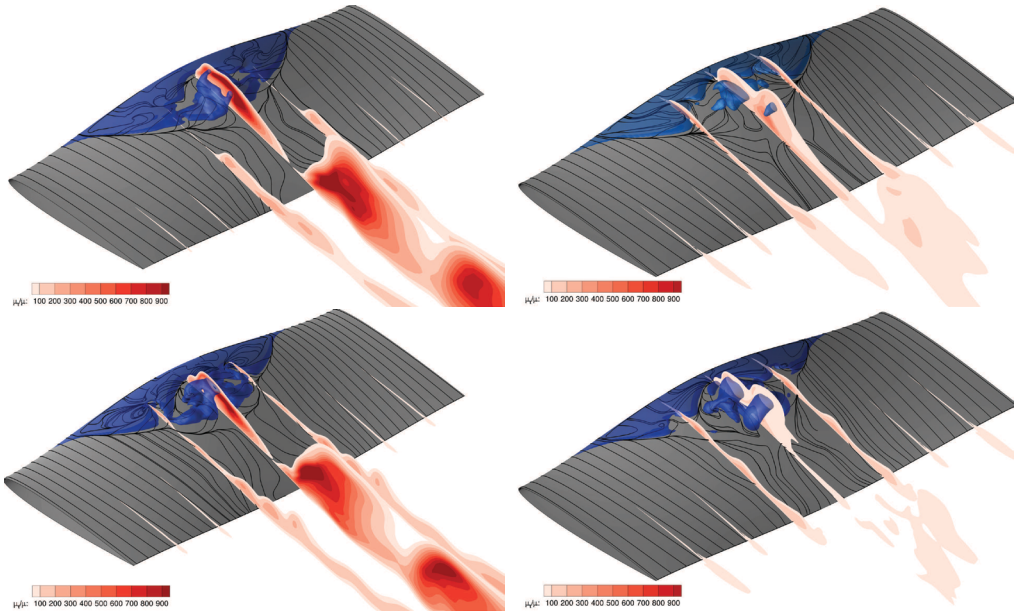

Figure 8: Cavity extent, limiting-streamlines and eddy-viscosity field. Instantaneous values. RANS-Reboud (left) and DDES (right); G4 (top) and G2 (bottom).

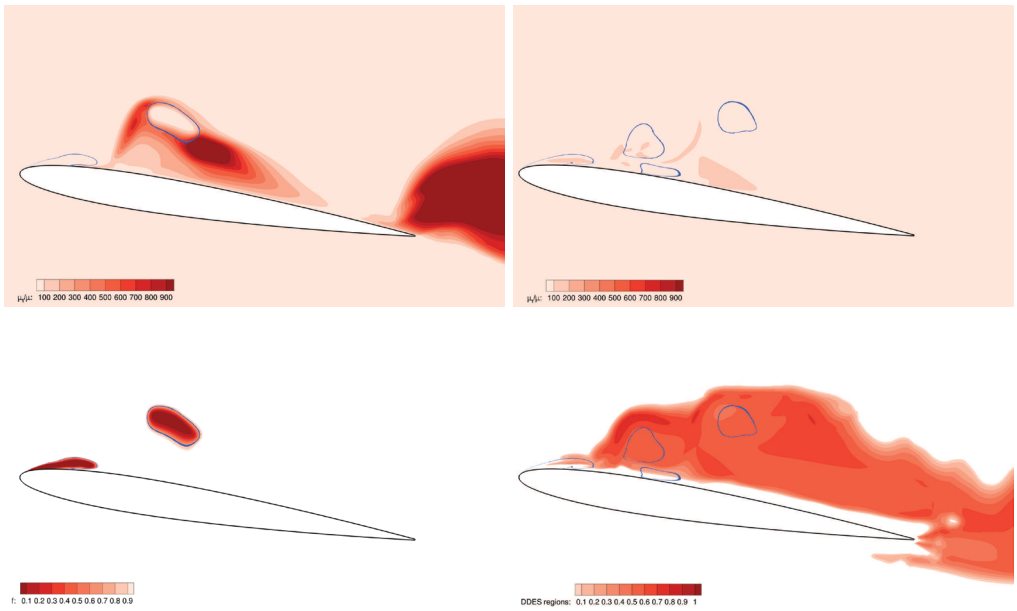

Figure 9: Eddy-viscosity $\frac{\mu_t}{\mu}$ (top), Reboud correction $\frac{f(\alpha)}{\rho}$ (bottom-left) and DDES activation $1 - \frac{l_t}{l_{RANS}}$ (bottom-right) fields. Instantaneous values on symmetry plane. RANS-Reboud (left) and DDES (right).

4.2.4 Comparison with experiments

Figure 10 shows the time-averaged C_p on the foil surface at the symmetry plane compared against experimental values [17]. One can clearly see that the RANS approach underpredicts the cavity length (and its dynamic behaviour) and that both RANS-Reboud and DDES deliver considerable improvements. There is a significant under-pressure area ($\sigma = 1.07$ in this case) both in the numerical calculations and experiments. Calculations underpredict the cavity length using all numerical approaches. Note that the predicted lift, even in wetted flow, is also too low when compared with the experiments, and therefore some uncertainty on these results is expected to be caused by the lower loading of the wing in the numerical calculations.

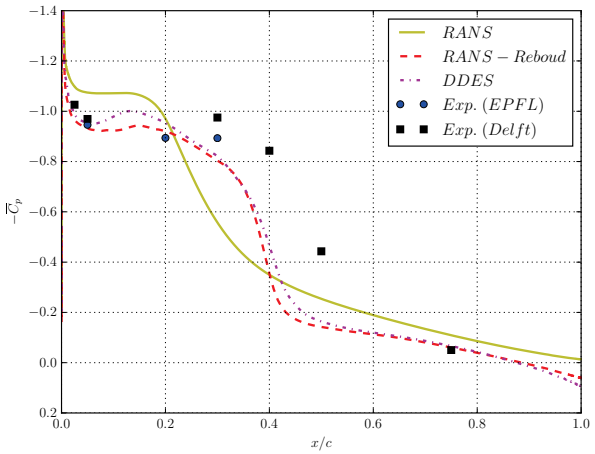

Figure 10: Time-averaged pressure coefficient on foil surface at $y/b = 0.5$ (midspan/symmetry plane) for RANS, RANS-Reboud and DDES.

Finally, Figure 11 illustrates for two time instants the comparison of the predicted cavity layouts with the experimental data available in [17]. These pictures demonstrate that the RANS-Reboud correction predicts the well established cavity re-entrant jet formation and upstream impinging flow, which is the origin of the cavity dynamic behaviour for this test-case. On the contrary, the DDES approach does not show this, and a more bulk vapour detachment external to the boundary-layer is seen. When compared with the experimental data, both numerical simulations underpredict the cavity length, volume and cloud cavitation formation. One can also notice that for these two instants the experiments show some asymmetry. While for RANS-Reboud the use of the complete wing is not expected to lead to different results, for an SRS approach like DDES this might have a measurable influence on the results.

5 CONCLUDING REMARKS

In this paper, we have analysed the differences between the application of a RANS, RANS including an eddy-viscosity (Reboud) correction and a DDES SRS approach for unsteady cavitation predictions on the 3D Delft "Twist11" Foil. We have examined these methods' quantitative accuracy both in terms of integral quantities and cavity dynamics, differing background principles, and the influence of grid refinement. The results obtained with these three approaches have been compared with experimental data and numerical results available in the literature.

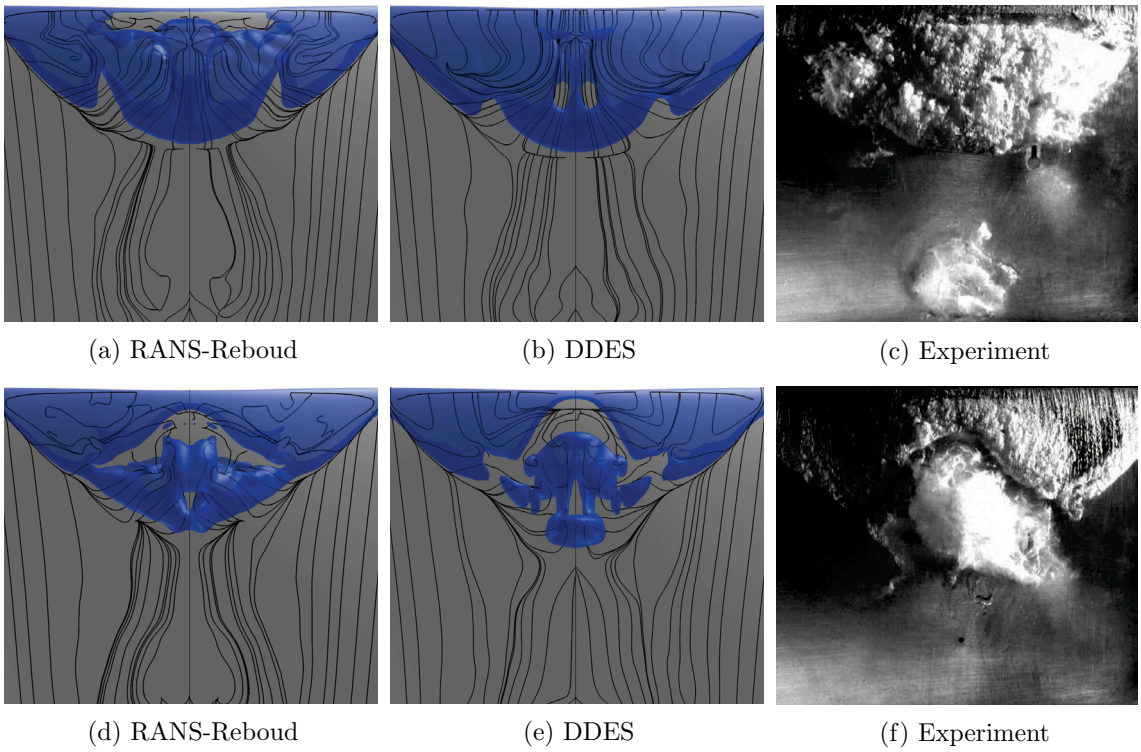

(a) RANS-Reboud (b) DDES (c) Experiment

(d) RANS-Reboud (e) DDES (f) Experiment

Figure 11: Cavity shape predicted using RANS-Reboud and DDES on G2 compared to experimental observations, at two different time instants. Top view, with cavity visualised as isosurface of $\alpha_v = 0.1$.

From the results presented one can draw the following conclusions:

- The numerical uncertainties for the wetted-flow calculations were small, the computational costs low and the iterative convergence optimal. Nevertheless, some differences between the numerical results and the reported experimental lift coefficient have been seen, which may indicate some discrepancies between the real experimental setup and the numerical setup here used, and by almost all authors that have addressed the same case.
- The grid design, utilising high-quality structured grids and locally nested refinement, increased the numerical resolution in the cavitation (and DDES) regions of interest. This is usually only done when employing unstructured grids.
- The numerical demands in terms of grids, time-step and non-linear iterations increase significantly in the case of cavitating-flow. For the RANS-Reboud correction case, these are even more significant. For the same numerical settings, DDES calculations delivered better iterative convergence at lower computational costs than the RANS-Reboud ones.
- The effect of grid refinement is different for all three methods used: 1) for RANS, the finer the grid the higher the values of eddy-viscosity and the worse the numerical predictions in

terms of cavity dynamics; 2) for DDES, the finer the grid the more turbulent structures are solved, the lower the eddy-viscosity levels, and the better the cavity dynamics; 3) for RANS-Reboud correction, refining the grid leads to non-monotonic convergence behaviour, which increases the numerical difficulties (robustness) of applying this correction.

- The cavity growth, shrinking and detachment was better captured using a RANS-Reboud correction approach than DDES. This is due to the shielding of the boundary layer from turbulence resolution intrinsic to this SRS model.
- The loads on the wing, and associated cavitation extents, were underpredicted when compared with the available experiments and some results of the literature.

In terms of future work, the authors would like to perform calculations for the same test case on finer grids, use the complete wing and study the effect of the time resolution. To employ other SRS methods like IDDES, XLES or PANS, or more advanced RANS turbulence models such as EARSM and RSM would also be the logical next step to improve the numerical predictions. Additionally, automatic grid and time-step adaptation (refinement and coarsening) would be a good technique to further reduce numerical dissipation, increase grid resolution in all vapour areas, and decrease the computational cost of these calculations.

ACKNOWLEDGMENTS

The authors would like to thank Maarten Kerkvliet and Bart Schuiling of MARIN for their help with the grid generation. This research is partially funded by the Dutch Ministry of Economic Affairs. This support is gratefully acknowledged.

References

[1] B. Ji, X. Luo, R. E. A. Arndt, and Y. Wu. Numerical simulation of three dimensional cavitation shedding dynamics with special emphasis on cavitationvortex interaction. *Ocean Engineering*, 87:64–77, 2014.

[2] D.-Q. Li and M. Grekula. Prediction of dynamic shedding of cloud cavitation on a 3D twisted foil and comparison with experiments. In *Proceedings of the 27th Symposium on Naval Hydrodynamics*, 5th-10th October, Seoul, Korea, 2008.

[3] R. E. Bensow. Simulation of the unsteady cavitation on the the Delft Twist11 foil using RANS, DES and LES. In *2nd International Symposium on Marine Propulsors*, Hamburg, Germany, 2011.

[4] O. Coutier-Delgosha, R. Fortes-Patella, and J. L. Reboud. Evaluation of the turbulence model influence on the numerical simulations of unsteady cavitation. *Journal of Fluids Engineering*, 125(1):38–45, 2003.

[5] M. Hoekstra, T. van Terwisga, and E. J. Foeth. SMP'11 Workshop - Case 1: DelftFoil. In *Second International Symposium on Marine Propulsors*, Hamburg, Germany, 2011.

[6] A. Asnaghi. *Developing computational methods for detailed assessment of cavitation on marine propellers*. Licentiate thesis, Chalmers University of Technology, 2015.

[7] N.-X. Lu. *Modelling Cavitation Mechanisms Using Large Eddy Simulation*. Ph.D. thesis, Chalmers University of Technology, 2013.

[8] B. Ji, X. W. Luo, R. E. A. Arndt, X. Peng, and Y. Wu. Large eddy simulation and theoretical investigations of the transient cavitating vortical flow structure around a NACA66 hydrofoil. *International Journal of Multiphase Flow*, 68:121–134, 2015.

[9] Y. Ait Bouziad. *Physical modelling of leading edge cavitation : computational methodologies and application to hydraulic machinery*. Ph.D. thesis, École Polytechnique Fédérale de Lausanne, 2005.

[10] E. J. Foeth, C. W. H. van Doorne, T. van Terwisga, and B. Wieneke. Time resolved PIV and flow visualization of 3D sheet cavitation. *Experiments in Fluids*, 40(4):503–513, 2006.

[11] F. R. Menter, Y. Egorov, and D. Rusch. Steady and unsteady flow modelling using the k-$\sqrt{k}$L model. In *Proceedings of the International Symposium on Turbulence, Heat and Mass Transfer*, Dubrovnik, Croatia, 2006.

[12] P. Perali, T. P. Lloyd, and G. Vaz. Comparison of uRANS and BEM-BEM for propeller pressure pulse prediction: E779A propeller in a cavitation tunnel. In *Proceedings of 19th Numerical Towing Tank Symposium*, 3rd-4th October, St. Pierre d'Oléron, France, 2016.

[13] M. S. Gritskevich, A. V. Garbaruk, J. Schütze, and F. R. Menter. Development of DDES and IDDES formulations for the k-ω shear stress transport model. *Flow, Turbulence and Combustion*, 88(3):431–449, 2012.

[14] G. H. Schnerr and J. Sauer. Physical and numerical modelling of unsteady cavitation dynamics. In *Proceedings of International Conference on Multiphase Flow*, New Orleans, USA, 2001.

[15] M. Hoekstra and G. Vaz. The partial cavity on a 2D foil revisited. In *Proceedings of 7th International Symposium on Cavitation*, 17th-22nd August, Michigan, USA, 2009.

[16] L. Eça and M. Hoekstra. A procedure for the estimation of the numerical uncertainty of CFD calculations based on grid refinement studies. *Journal of Computational Physics*, 262:104–130, 2014.

[17] E. J. Foeth. *The structure of three-dimensional sheet cavitation*. Ph.D. thesis, TU Delft, 2008.